Electronic Supplementary Information

A series of lanthanide−organic frameworks possessing arrays of 2D intersecting channels within a 3D pillar-supported packed double-decker network and Co^{2+}-induced luminescence modulation†

Yen-Hsiang Liu*, Po-Hsiu Chien

Department of Chemistry, Fu Jen Catholic University,
New Taipei City 24205, Taiwan.

Keywords: Lanthanide–organic frameworks / Sensors / Tunable photoluminescence / Selectivity

*Corresponding author: e-mail: *056461@mail.fju.edu.tw* (Y.-H. Liu)

Photoluminescence measurements

The photoluminescence (PL) spectra of 2,6-NDC, **Eu-FJU6**, desolvated **Eu-FJU6**, and inclusion samples were recorded on a Perkin-Elmer LS55 flurorescence spectrometer at room temperature with the identical light source and scan rate of 200 nm/min. The respective detector voltage, emission filter, excitation and emission slit width for their maximum intensity of excitation and emission band are listed as follows:

(a) 2,6-NDC ligand	(b) as-synthesized, desolvated **Eu-FJU6**, and guest-inclusion samples
Light source: Fluorescence	Light source: Fluorescence
Slit width (ex,em)[a]: (5 nm, 2.5 nm)	Slit width (ex,em)[a]: (5.2 nm, 2.6 nm)
Scan rate: 200nm/min	Scan rate: 200nm/min
Emission filter: 350 nm	Emission filter: 350 nm
Photomultiplier type: R928	Photomultiplier type: R928
Detector voltage: 650 V	Detector voltage: 750 V

[a] ex = excitation; em = emission.

PXRD and IR properties of desolvated Eu-FJU6

As shown in Fig. S1, the observable new phases along with distortions happening to the structure of desolvated **Eu-FJU6** suggested that distinct crystal lattice was formed. This phenomenon of shift, broadening, appearance, or emergence of diffraction lines was well-known for lanthanide ─ organic frameworks due to susceptible metal coordination spheres.[1] On the basis of the literature,[2] it was highly of possibility that the lowering of symmetry of desolvated **Eu-FJU6** and structural distortions were induced by the carboxylate shift within the host thick-floors frameworks. It was worth noting, however, that the evacuation of guest molecules brought about a certain extent of distortions, the microporosity remained nearly intact as evidenced by the expanded spacing between the planes in the crystal lattice. Furthermore, attempts to confirm the in situ-generated active Eu^{3+} sites revealed no characteristic absorptions for the carbonyl vibrations of DMF molecules (1668 cm^{-1}), since hydrolysis of coordinated DMF molecules along with thermal decarbonylation led to the formation of dimethylammonium cations.[3] More importantly, strong absorptions for the symmetric and asymmetric vibrations of $Eu-O_{carboxylate}$ bonds at 1650 ─ 1550 cm^{-1} and 1420 ─ 1335 cm^{-1} indicated that the host thick-floors frameworks was retained after the evacuation of guest molecules. Taking the absorption peaks and phase integrity into account, we furthered studies as to sensing with desolvated **Eu-FJU6**.

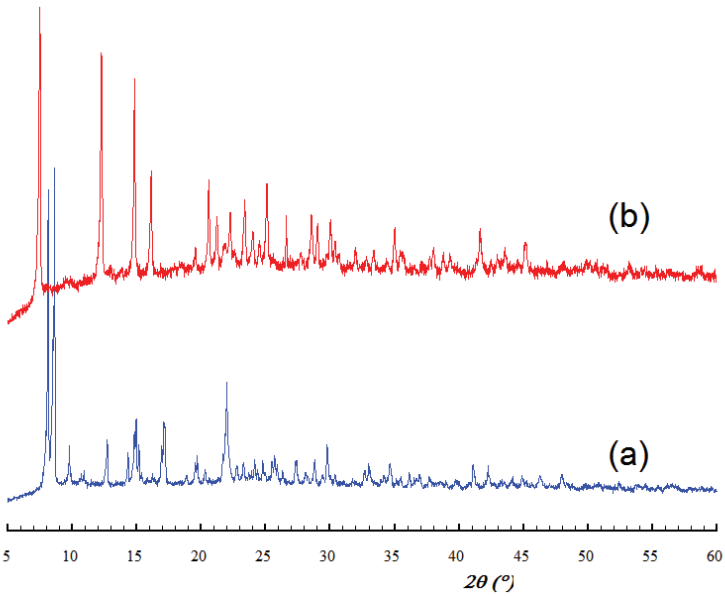

Figure S1. Powder X-ray diffraction patterns: (a) as-synthesized **Eu-FJU6**; (b) desolvated sample of **Eu-FJU6**.

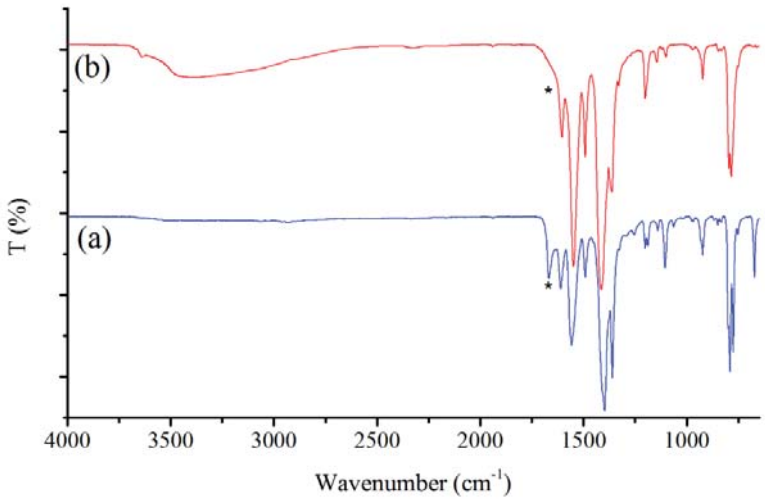

Figure S2. IR spectra: (a) simulated; (b) desolvated sample of **Eu-FJU6** (* represents the absorption peak of $-C=O_{DMF}$ bond).

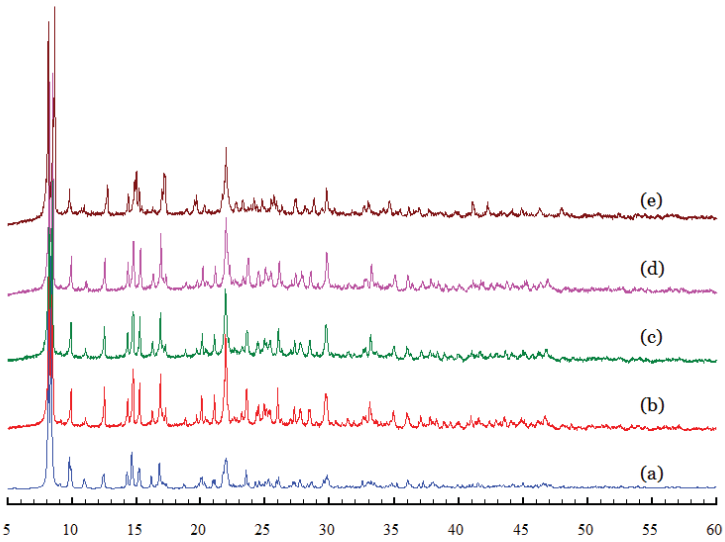

Figure S3. Powder X-ray diffraction patterns of: (a) simulated; (b) **Ce-FJU6**; (c) **Pr-FJU6**; (d) **Nd-FJU6**; (e) **Eu-FJU6** samples.

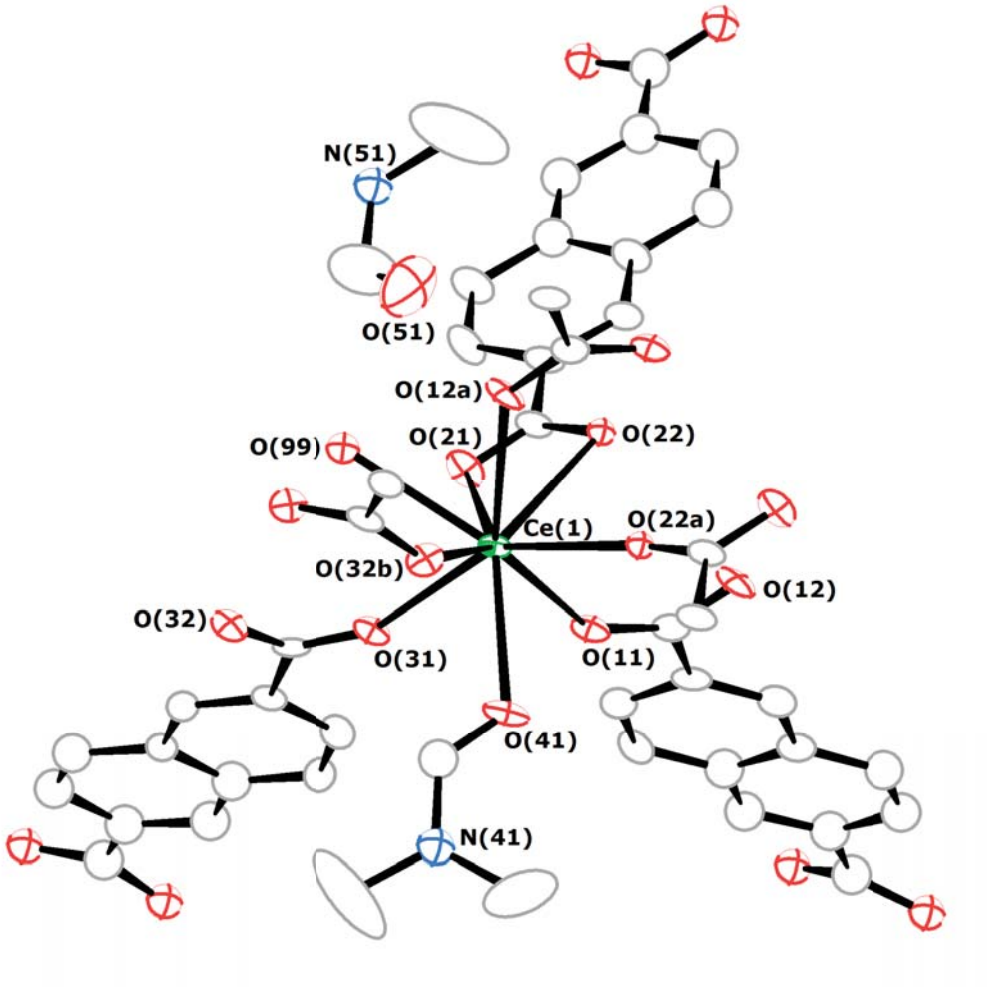

Figure S4. Atom numbering scheme of **Ce-FJU6**[a] in the crystallographic asymmetric unit with ellipsoids are shown at the 30% level. [a] Symmetry transformations used to generate equivalent atoms: (a) *2 − x*, *− y*, *− z*; (b) *2 − x*, *y*, *0.5 − z*. Key: green, Ce; gray, C; red, O; blue, N; all the H atoms are omitted for clarity.

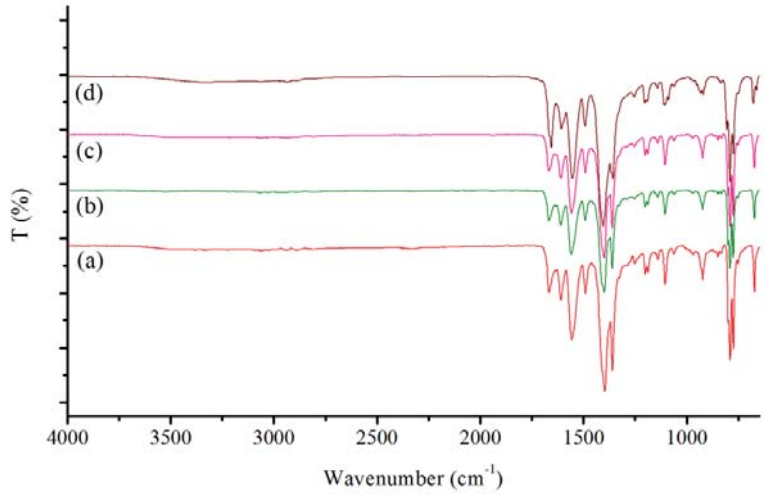

Figure S5. IR spectra of: (a) **Ce-FJU6**; (b) **Pr-FJU6**; (c) **Nd-FJU6**; (d) **Eu-FJU6** samples**.**

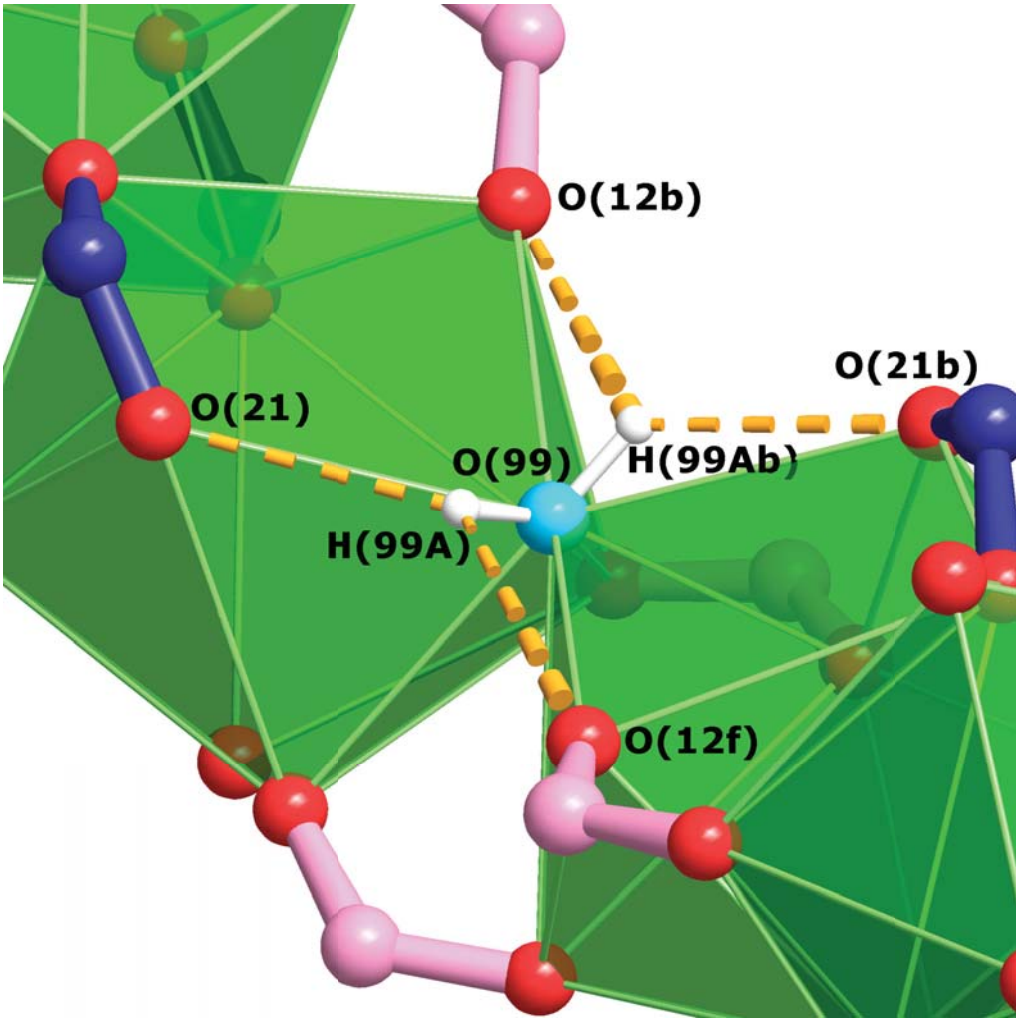

Figure S6. Moderate hydrogen-bonding interactions of **Ce-FJU6**[a] from between the bridged water molecules to the carboxylate oxygen atoms. [a]Symmetry transformations used to generate equivalent atoms: (b) *2 – x*, *y*, *0.5 – z*; (f) *x*, *– y*, *0.5 + z*. Key: green, Ce; pink, C in NDC^{I}; darkblue, C in NDC^{II}; red, O; aqua, O in water molecule; white: H.

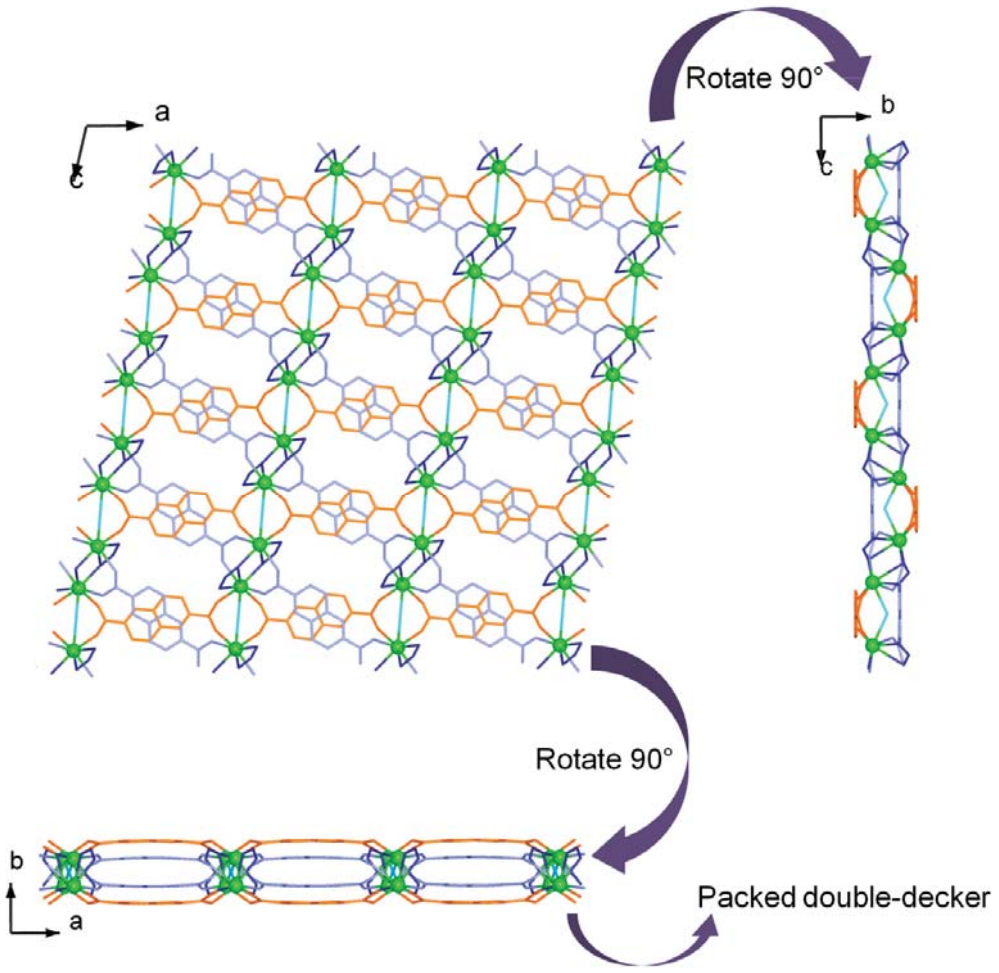

Figure S7. The illustration of a packed 2D double-decker as viewed along the *a*-, *b*-, and *c*-direction.

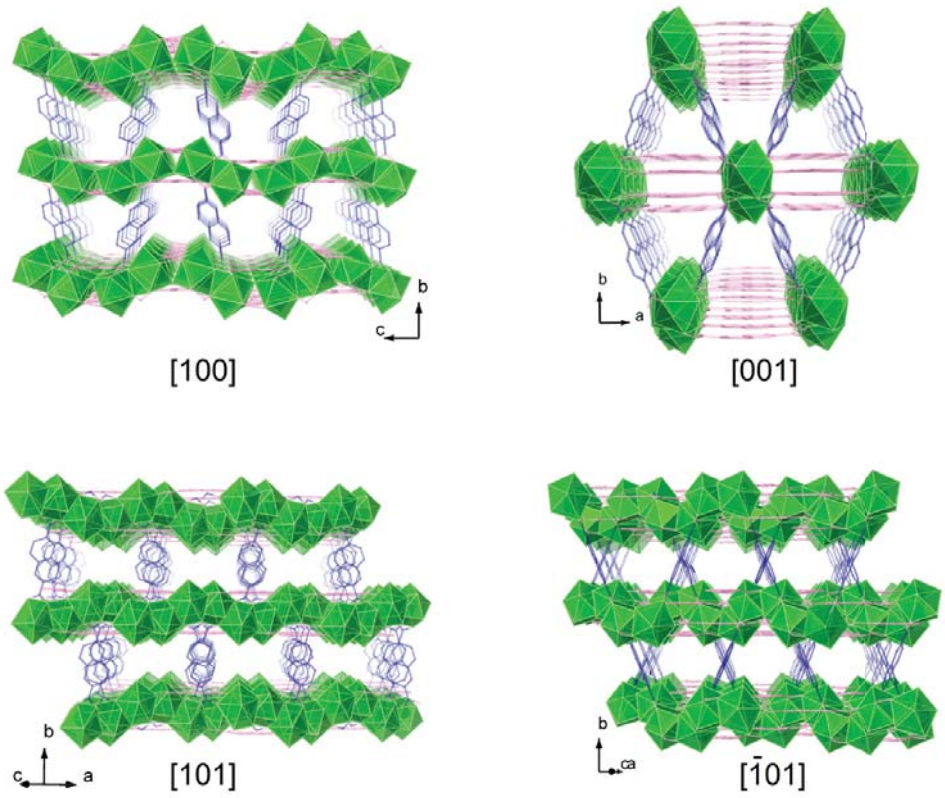

Figure S8. Perspective views of 1D porous channels along the four different directions. Key: green, Ce; pink, C in NDC^{I}; darkblue, C in NDC^{II}; red, O; aqua, O in water molecule; all the H atoms are omitted for clarity.

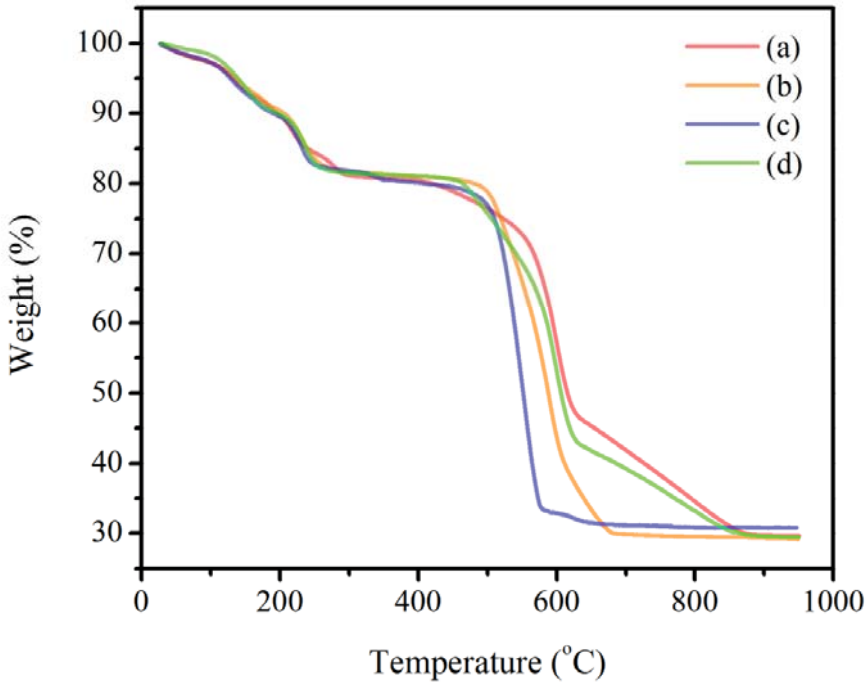

Figure S9. Thermogravimetric curves of: (a) **Ce-FJU6**; (b) **Pr-FJU6**; (c) **Nd-FJU6**; (d) **Eu-FJU6** samples**.**

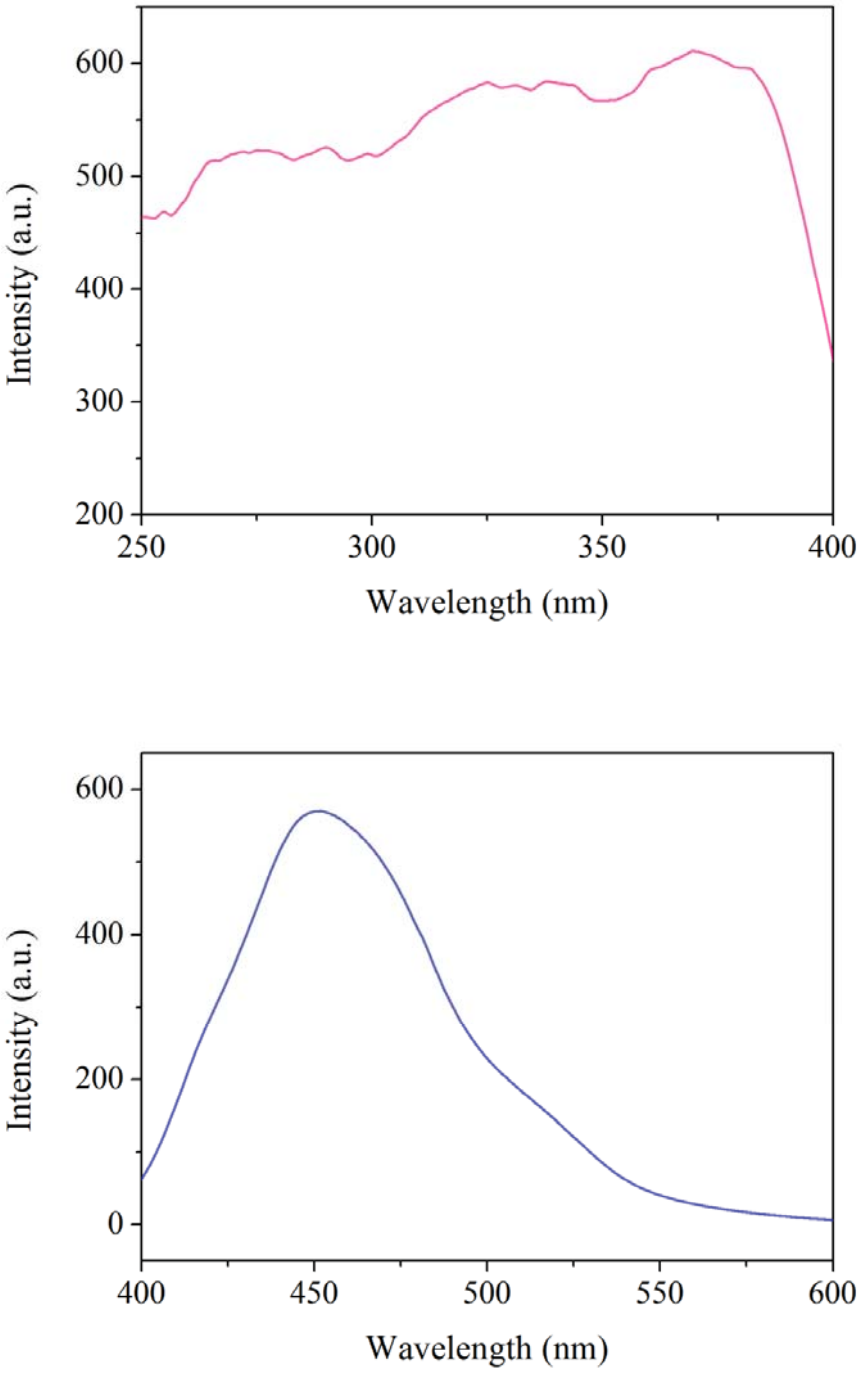

Figure S10. Excitation (top) and photoluminescence spectra (bottom) of 2,6-NDC ligand.

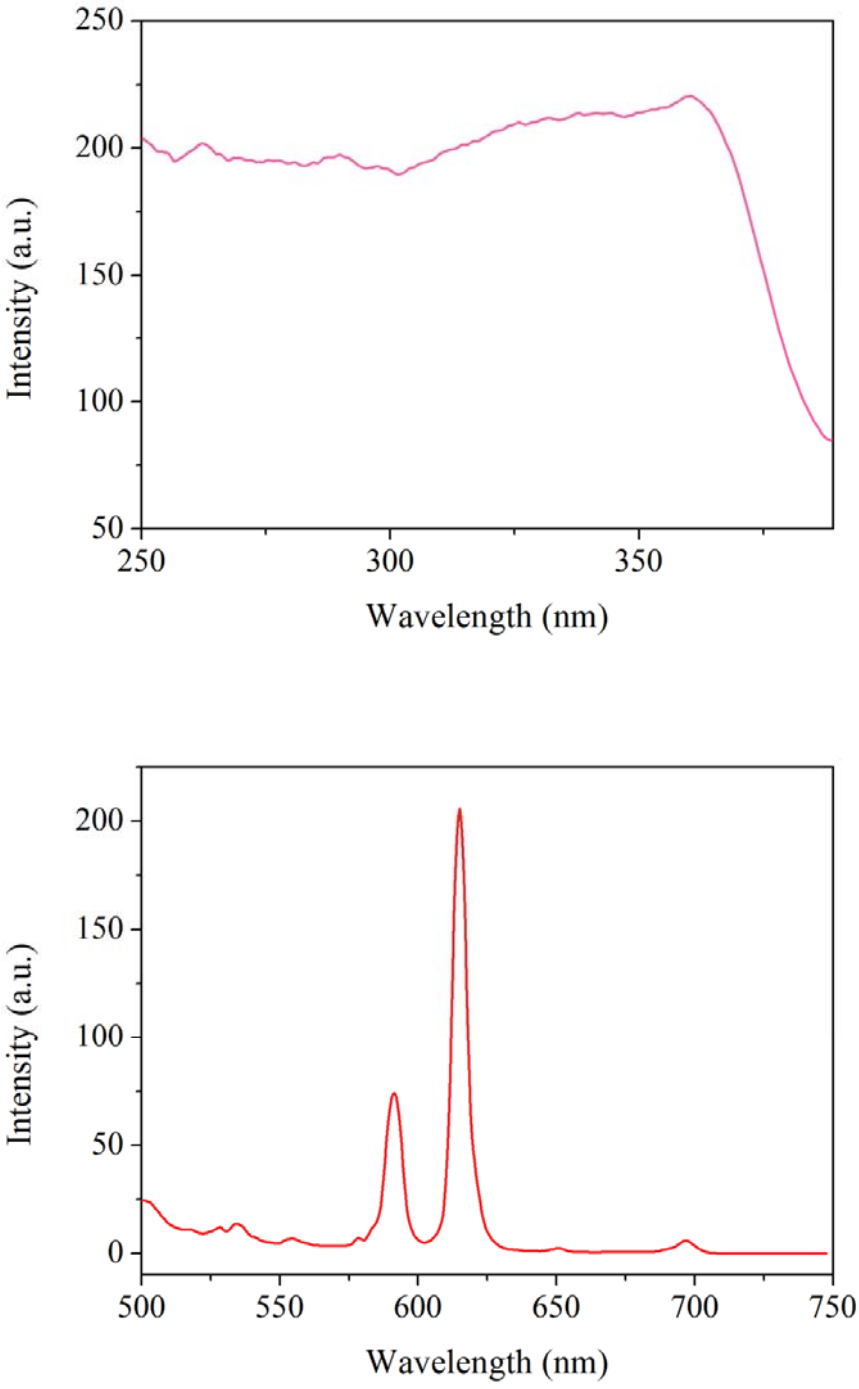

Figure S11. Excitation (top) and photoluminescence spectra (bottom) of desolvated **Eu-FJU6**.

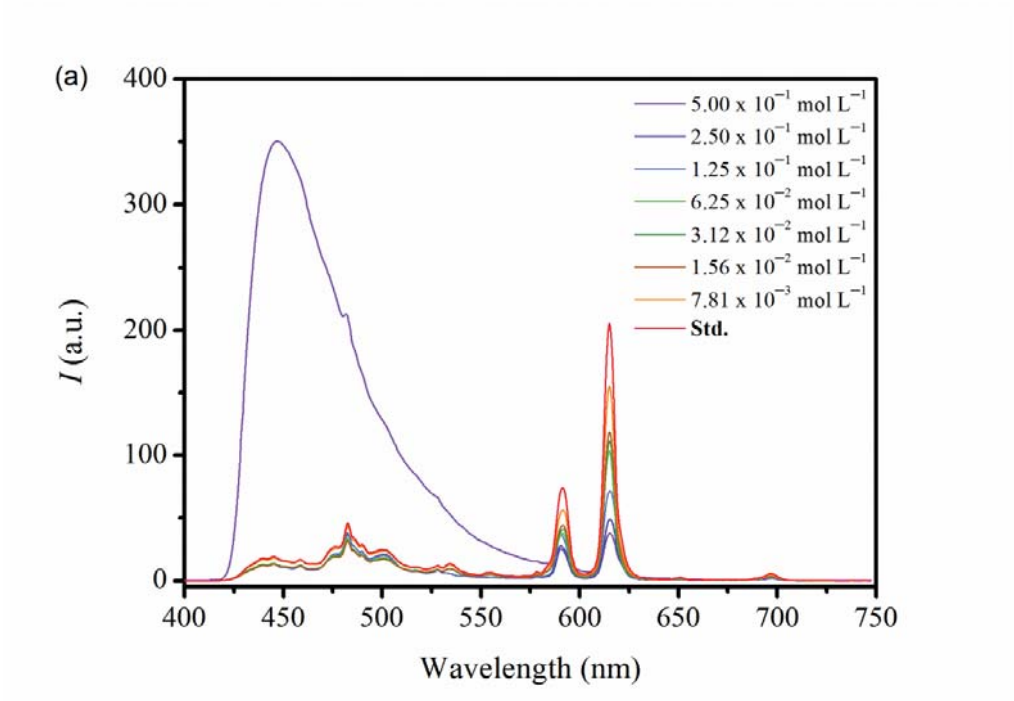

Fig. **S12**. (a) PL spectra of **Eu-FJU6**⊃Ni^{2+} in various concentrations when excited at 368 nm (**Std**.: represents desolvated **Eu-FJU6**).

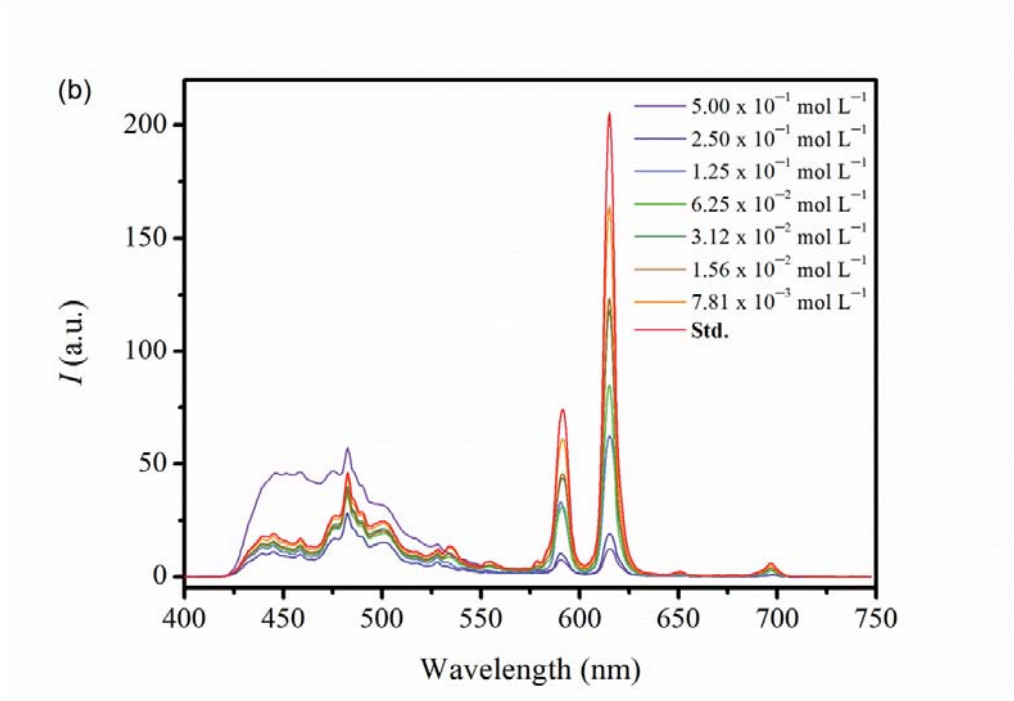

Fig. **S12**. (b) PL spectra of **Eu-FJU6**⊃Co^{2+} in various concentrations when excited at 368 nm (**Std**.: represents the desolvated **Eu-FJU6**).

PXRD and photoluminescence properties of cation-inclusion Eu-FJU6 (Eu-FJU6⊃cation)

Regarding the PXRD analysis of the inclusion sample **Eu-FJU6**⊃cation (Fig. S13), only patterns of **Eu-FJU6**⊃Ni^{2+} and **Eu-FJU6**⊃Co^{2+} microcrystalline powder were perfect matches for the desolvated **Eu-FJU6**, verifying that the 3D thick-floor frameworks are suitable for exploring the Metal–Lewis basic carboxylate site interactions, since no additional structural distortions were observed. In contrast, the severe shift, broadening, appearance, or emergence of diffraction peaks revealed the fact that the microporosity of the other inclusion samples such as **Eu-FJU6**⊃Cu^{2+}, **Eu-FJU6**⊃Zn^{2+}, and **Eu-FJU6**⊃Cd^{2+} had undergone further deconstruction after desolvation.

As shown in Fig. S14~15, the luminescence intensity of the Eu^{3+}-based emission in **Eu-FJU6**⊃Cu^{2+}, **Eu-FJU6**⊃Zn^{2+}, and **Eu-FJU6**⊃Cd^{2+} essentially completely disappeared as the concentration of Cu^{2+}, Zn^{2+}, and Cd^{2+} ions were adjusted to 0.5 mol L^{-1} or 0.25 mol L^{-1}. As expected, a broad hump at 425–625 nm, which can be assigned to the ligand centered emission band of 2,6-NDC, was observed in **Eu-FJU6**⊃Cu^{2+}, **Eu-FJU6**⊃Zn^{2+}, and **Eu-FJU6**⊃Cd^{2+} (with the identical set of photoluminescence measurements, a few emission bands of blue light in the inclusion samples were so strong that the intensity was beyond the detection limit of the spectrometer), indicating the network symmetry of the 3D thick-floor frameworks of **Eu-FJU6**⊃Cu^{2+}, **Eu-FJU6**⊃Zn^{2+}, and **Eu-FJU6**⊃Cd^{2+} were distorted to a lower symmetry more severely than that of **Eu-FJU6**⊃Ni^{2+}**, Eu-FJU6**⊃Co^{2+}, as mentioned above. In addition, the moderate blue light emitted by **Eu-FJU6**⊃Ni^{2+} (Fig. S14a) further verified that the perturbation, which is due to the inefficient ligand-to-metal energy transfer, of the coordination spheres of Eu^{3+} ions was possibly caused by concentrated Ni^{2+} ions, even though the PXRD pattern of **Eu-FJU6**⊃Ni^{2+} was in good agreement with that for the desolvated form of **Eu-FJU6** (Fig. S13). Hence, we speculate that Cu^{2+}, Zn^{2+}, Cd^{2+}, and concentrated Ni^{2+} ions interfere heavily with the ligand-to-metal energy transfer from the 2,6-NDC sensitizers to Eu^{3+} centers in the desolvated **Eu-FJU6**.

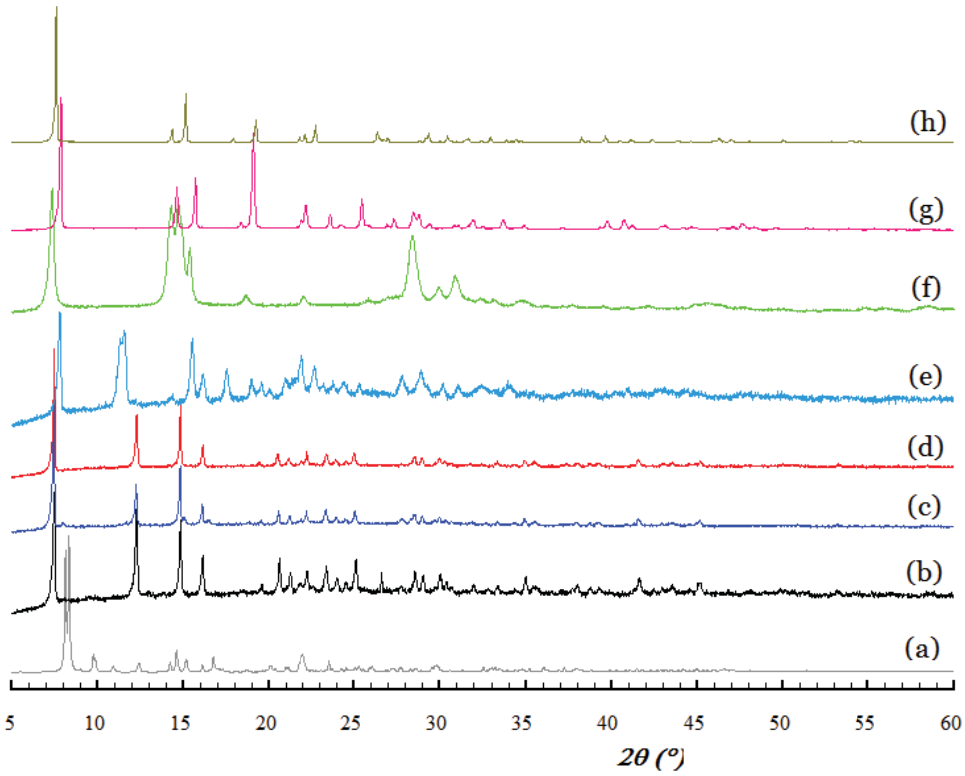

Figure S13. Powder X-ray diffraction patterns of: (a) simulated; (b) desolvated **Eu-FJU6**; (c) **Eu-FJU6**⊃Ni^{2+}; (d) **Eu-FJU6**⊃Co^{2+}; (e) **Eu-FJU6**⊃Na^{+}; (g) **Eu-FJU6**⊃Cu^{2+}; (h) **Eu-FJU6**⊃Zn^{2+}; (i) **Eu-FJU6**⊃Cd^{2+} samples.

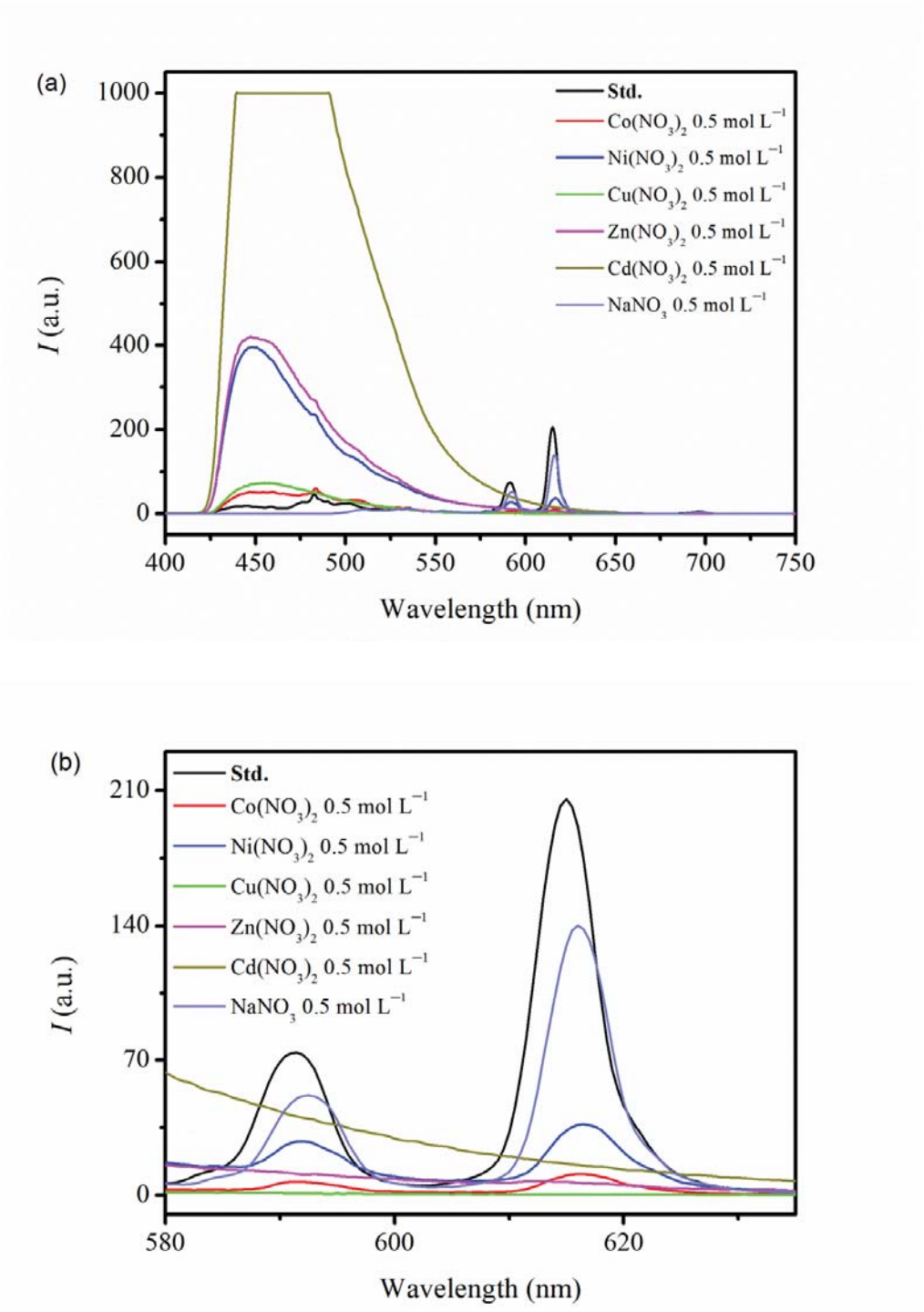

Fig. S14. (a) An enormous emission band at ~452 nm based on $\pi^* - \pi$ transition of NDC^{2-} ligands was observed in **Eu-FJU6**⊃Ni^{2+}, **Eu-FJU6**⊃Zn^{2+} and **Eu-FJU6**⊃Cd^{2+} (λ_{ex} = 368 nm); (b) The comparison of PL intensity focused on the $^5D_0 \rightarrow {}^7F_1$ and $^5D_0 \rightarrow {}^7F_2$ transitions of Eu^{3+} ions in inclusion samples

Eu-FJU6⊃cation with different metal ions in 0.5 mol L^{-1} when excited at 368 nm. (**Std**.: represents the desolvated **Eu-FJU6**).

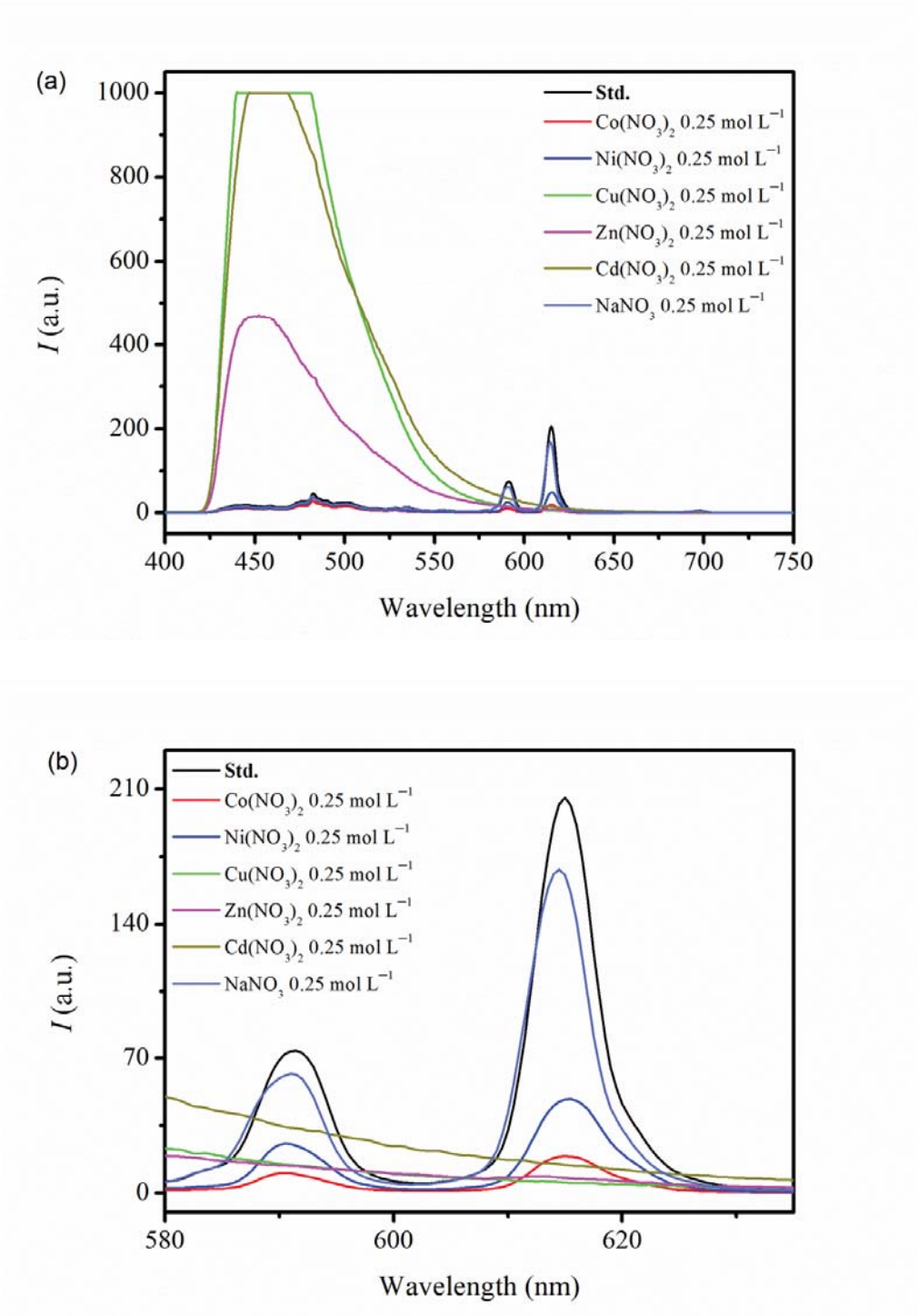

Fig. S15. (a) An enormous emission band at ~452 nm based on $\pi^* - \pi$ transition of NDC^{2-} ligands was observed in **Eu-FJU6**⊃Cu^{2+}, **Eu-FJU6**⊃Zn^{2+} and **Eu-FJU6**⊃Cd^{2+}, whereas the IL band was completely vanished in **Eu-FJU6**⊃Ni^{2+} (λ_{ex} = 368 nm); (b) The comparison of PL intensity focused on the $^5D_0 \rightarrow {}^7F_1$ and $^5D_0$

$\rightarrow {}^{7}F_2$ transitions of Eu^{3+} ions in **Eu-FJU6**⊃cation with different metal ions in 0.25 mol L^{-1} when excited at 368nm. (**Std**.: represents the desolvated **Eu-FJU6**).

Reference:

1 (a) D. W. Breck, *Zeolite*, *Molecular Sieves*, *Structure*, *Chemistry*, *and Use*, John Wiley & Sons, 1974; (b) T. M. Reineke, M. Eddaoudi, M. Fehr, D. Kelley and O. M. Yaghi, *J. Am. Chem. Soc*., 1999, **121**, 1651; (c) F. Luo and S. R. Batten, *Dalton*, *Trans*., 2010, **39**, 4485.

2 (a) R. L. Rardin, A. Bino, P. Poganiuch, W. B. Tolman, S. Liu and S. J. Lippard, *Angew. Chem*., *Int. Ed*., 1990, **29**, 812; (b) X.-M. Chen and T. C. W. Mark, *Inorg. Chem*., 1994, **33**, 2444; (c) D.-X. Xue, W.-X. Zhang, X.-M. Chen and H.-Z. Wang, *Chem. Commun*., 2008, 1551; (d) B. Chen, L. Wang, Y. Xiao, F. R. Fronczek, M. Xue, Y. Cui and G. Qian, *Angew. Chem*., *Int. Ed*., 2009, **48**, 500.

3 (a) S. M. Hawxwell and L. Brammer, *CrystEngComm*, 2006, **8**, 473; (b) A. D. Burrows, K. Cassar, R. M. W. Friend, M. F. Mahon, S. P. Rigby and J. E. Warren, *CrystEngComm*, 2005, **7**, 548.